

# Oscillator strengths, Huang–Rhys parameters, and vibrational quantum energies of cerium-doped gadolinium oxyorthosilicate

D. W. Cooke,<sup>a)</sup> B. L. Bennett, K. J. McClellan, J. M. Roper, and M. T. Whittaker  
*Materials Science and Technology Division, Los Alamos National Laboratory, Los Alamos, New Mexico 87545*

(Received 29 November 1999; accepted for publication 15 February 2000)

Temperature-dependent optical absorption of cerium-doped gadolinium oxyorthosilicate ( $\text{Gd}_2\text{SiO}_5\text{:Ce}$ ) has been measured and analyzed for impurity-ion-lattice coupling parameters and oscillator strengths. Although the spectrum consists of overlapping  $\text{Ce}^{3+}$  bands and  $\text{Gd}^{3+}$  lines, two well-resolved  $\text{Ce}^{3+}$  bands with 10 K maxima at 3.32 eV (peak a) and 3.61 eV (peak b) are amenable to spectral analysis. These bands, previously assigned to  $\text{Ce}^{3+}$  ions occupying crystallographically inequivalent substitutional sites, are characterized by Gaussian line shapes and temperature-dependent half widths that are well described by the linear model of impurity-ion-lattice coupling. Huang–Rhys [Proc. R. Soc. A **204**, 404 (1950)] parameters of peaks a and b are 22.7 and 5.7, respectively, indicating strong ion-lattice coupling, with vibrational frequencies  $1.83 \times 10^{13} \text{ s}^{-1}$  (peak a) and  $5.07 \times 10^{13} \text{ s}^{-1}$  (peak b). Peak b centroid is approximately temperature independent, but peak a centroid shifts to higher energy with increasing temperature. This dependence is adequately described by including higher-order coupling terms in the ion-lattice interaction, although crystal-field contributions cannot be excluded. Absorption band oscillator strengths,  $f$ , are calculated from Smakula's [Z. Phys. **59**, 603 (1930)] formula and knowledge of cerium concentration for the two inequivalent sites. In the interval 10–300 K, peak a  $f$  values range from  $(9.8 \text{ to } 26.8) \times 10^{-4}$  and peak b  $f$  values vary from  $(7.8 \text{ to } 5.8) \times 10^{-3}$ . From the known correlation between oscillator strength and metal-ion-ligand separation, we identify peaks a and b as the seven- and nine-oxygen-coordinated sites, respectively. © 2000 American Institute of Physics. [S0021-8979(00)02011-9]

## I. INTRODUCTION

Cerium-doped gadolinium oxyorthosilicate,  $\text{Gd}_2\text{SiO}_5\text{:Ce}$  (GSO), is an efficient scintillator characterized by relatively high quantum efficiency, high density ( $6.71 \text{ g/cm}^3$ ), and large effective atomic number (59).<sup>1</sup> A typical emission spectrum consists of a band with maximum near 430 nm, which is attributed to the  $5d \rightarrow 4f$  electronic transitions of the  $\text{Ce}^{3+}$  ions.<sup>2</sup> However, the luminescence decay, comprised of two lifetime components ( $\sim 56$  and  $600 \text{ ns}$ ), is much slower than expected from the usual prompt deexcitation of the  $\text{Ce}^{3+}$  ions ( $\sim 25 \text{ ns}$ ) and likely involves resonant energy transfer between the  $\text{Ce}^{3+}$  and  $\text{Gd}^{3+}$  ions.<sup>3,4</sup> Further complexity of the fundamental luminescence mechanism arises from the fact that GSO has two crystallographically inequivalent sites for  $\text{Ce}^{3+}$  ions with each one exhibiting distinct temperature- and concentration-dependent emission and excitation spectra.<sup>5</sup> By comparing optical excitation, absorption, and emission spectra, Suzuki *et al.*<sup>5</sup> correlated the prominent features in the optical absorption spectrum of GSO with sites Ce1, Ce2, and  $\text{Gd}^{3+}$ . The specific site designation (Ce1 and Ce2) arises from the fact that crystalline GSO is known to possess monoclinic symmetry with space group  $P2_1/c$  with  $\text{Gd}^{3+}$  ions occupying two crystallographically inequivalent sites coordinated with either seven or nine oxygens.<sup>6</sup> Pre-

sumably  $\text{Ce}^{3+}$  incorporation into the host lattice occurs via substitution for  $\text{Gd}^{3+}$  and thus should also occupy two inequivalent sites, arbitrarily denoted as Ce1 and Ce2. The correlation of Ce1 and Ce2 with specific oxygen-coordinated sites has not yet been established. Moreover, fundamental impurity-ion-lattice coupling parameters and oscillator strengths of the optical transitions, which should prove useful in elucidating the fundamental luminescence mechanism and identifying the oxygen-coordinated sites, have not been reported.

In this article, we present results of ultraviolet and visible (uv-vis) optical absorption measurements on single-crystal GSO made in the temperature interval 10–300 K. Analysis of the data yields oscillator strengths, vibrational quantum energies, and Huang–Rhys parameters of the prominent absorption bands. Knowledge of the cerium concentration of sites Ce1 and Ce2, coupled with the known correlation of Ce-ion-ligand distance with oscillator strength, allows assignment of Ce1 and Ce2 to the nine and seven-oxygen-coordinated sites, respectively.

## II. EXPERIMENT

A single crystal of GSO, provided by Hitachi Chemical Company, was fabricated into sample dimensions  $1 \times 1 \times 0.026 \text{ cm}^3$  and polished to a surface finish of  $3 \mu\text{m}$ . Cerium concentration in the growth melt was 0.25 at. % relative to  $\text{Gd}^{3+}$ , but due to the smaller size of the  $\text{Gd}^{3+}$  ion (0.938

<sup>a)</sup> Author to whom correspondence should be addressed; electronic mail: cooke@lanl.gov

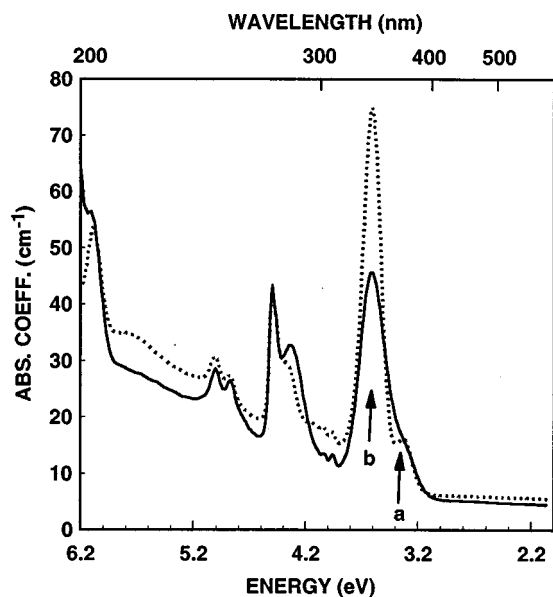


FIG. 1. Optical absorption of GSO measured at 300 K (solid line) and 10 K (dotted line). The ordinate refers to the decadic absorption coefficient  $\alpha$  of the 0.026-cm-thick sample. Arrows denote peaks of the two principal absorption bands a and b.

$\text{\AA}$ ) relative to  $\text{Ce}^{3+}$  (1.034  $\text{\AA}$ ), the final sample concentration was lower. Using the known crystal-to-melt distribution coefficient 0.6 yields a final  $\text{Ce}^{3+}$  concentration of 0.15 at. %.<sup>7</sup>

A Cary 5E optical absorption spectrophotometer, modified to accommodate an optical cryostat, was used to obtain uv-vis data in the temperature range 10–300 K. Absorption spectra were taken at 10 and 20 K, and at each 20 K interval thereafter up to 300 K. To ensure thermal equilibrium between the sample and cold finger, the specimen was held at each set point for 10 min prior to recording the absorption spectrum. Sample temperature was measured with a carbon-glass resistor and controlled to within  $\pm 2$  K of the set point by a LakeShore Cryotronics Model 340 temperature controller. Spectral data were recorded in absorbance units as a function of wavelength and plotted as decadic absorption coefficient  $\alpha$  ( $=0.4343 \kappa$ , where  $\kappa$  is the absorption coefficient to base  $e$ ) vs photon energy. Fitting of the absorption bands to known spectral shapes was done with a commercial software package utilizing the Levenberg–Marquardt nonlinear least-squares routine.

### III. RESULTS AND DISCUSSION

#### A. Peak shape determination

Figure 1 shows the optical absorption spectra of GSO taken at 300 K (solid line) and 10 K (dotted line), with the principal peaks denoted by arrows a and b, in excellent agreement with the previously reported results of Suzuki *et al.*<sup>5</sup> These researchers compared GSO excitation and emission spectra and concluded that two types of cerium centers were involved in the emission process. One center, arbitrarily designated Ce1, exhibited excitation and absorption bands at 284 nm (4.36 eV) and 345 nm (3.59 eV), with corresponding emission maximum near 425 nm (2.92 eV). The other center, arbitrarily denoted Ce2, was characterized

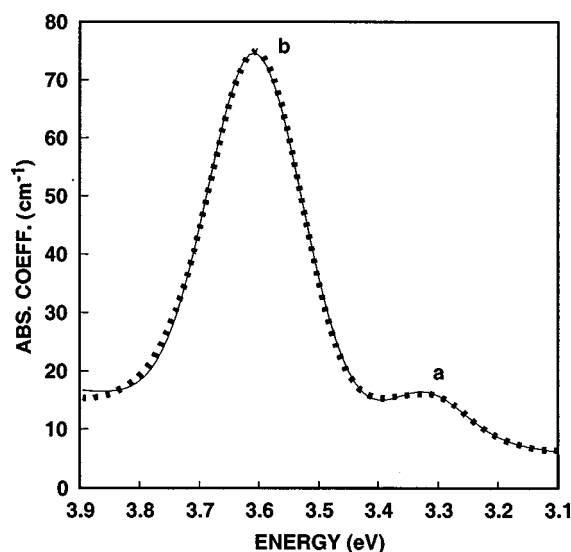


FIG. 2. Experimental, 10 K absorption spectrum of GSO plotted on a reduced energy scale (dotted line). The thin solid line represents a composite fit obtained by adding two Gaussians that best fit the individual bands a and b.

by excitation bands at 300 nm (4.13 eV) and 378 nm (3.28 eV), an absorption band at 378 nm and possibly one at 300 nm, with emission maximum near 480 nm (2.58 eV). Note that in the present data, we do not observe a distinct peak near 4.13 eV, but instead see the appearance of at least two small peaks in this vicinity. Additional absorption lines with maxima at 4.51, 4.92, and 5.02 eV were assigned by Suzuki *et al.*<sup>5</sup> to optical transitions of the  $\text{Gd}^{3+}$  ions. The overlap of  $\text{Gd}^{3+}$  line emission with the  $\text{Ce}^{3+}$  band emission precludes straightforward analysis of absorption bands other than the principal ones labeled a and b in Fig. 1. These latter bands are our main interest because they purportedly belong to different cerium sites and are of sufficient intensity and resolution to be amenable to analysis, thus allowing a comparison of oscillator strengths and impurity-ion-lattice coupling parameters for the two inequivalent cerium sites. Therefore, we confine our analysis to these two principal bands.

The dotted line of Fig. 2 shows the experimental, 10 K absorption spectrum of GSO plotted on a reduced energy scale to highlight the main peaks. The thin solid line is a composite fit obtained by adding two Gaussian bands, each representing the best fit to individual bands a and b. Attempts to fit these bands with Lorentzian or Voigt line shapes at any temperature in the interval 10–300 K were unsuccessful. The best fits at 10 K were obtained with Gaussian line shapes exhibiting maxima at 3.32 eV (peak a) and 3.61 eV (peak b) with reduced  $\chi^2=0.9992$  (reduced  $\chi^2$  is the square of the difference between the actual and calculated values divided by the number of degrees of freedom). The statistical errors in these values, derived from the fitting routine, are less than  $10^{-5}$  eV and the experimental spectral resolution is  $\pm 0.5$  nm. Similar high-quality Gaussian fits were obtained for these two bands over the temperature interval investigated, from which spectral moments and areas were extracted.

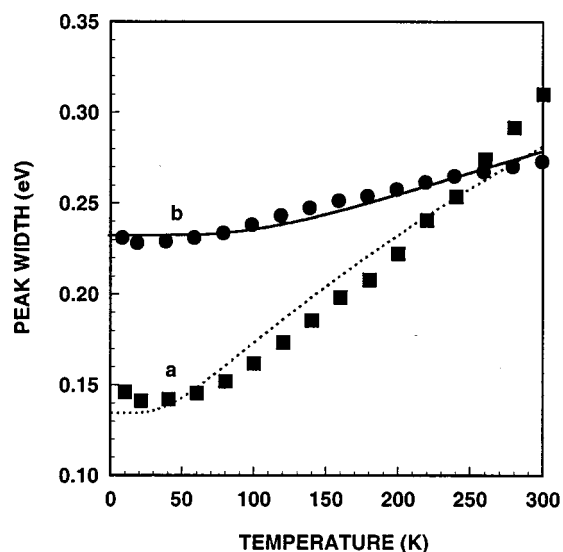


FIG. 3. Temperature dependence of the peak widths, i.e., full width at half maximum, of the principal absorption bands a and b. Solid and dotted lines represent the best fits of the data to the linear, ion-lattice interaction model.

### B. Vibrational quantum energies and Huang-Rhys parameters

Configuration-coordinate diagrams are convenient for describing optical absorption and emission processes in solids.<sup>8</sup> In this model, the ground and excited states of the impurity center are described as classical quantum-mechanical oscillators with quantum energy  $\hbar\omega$ , leading to the prediction that the full width at half maximum,  $W(T)$ , of the optical absorption band varies with temperature according to the relation

$$W(T) = W(0) \left[ \coth \left( \frac{\hbar\omega}{2kT} \right) \right]^{1/2}. \quad (1)$$

For Gaussian line shapes, this can be expressed as

$$W(T) = \hbar\omega \left[ 8S \ln 2 \coth \left( \frac{\hbar\omega}{2kT} \right) \right]^{1/2}, \quad (2)$$

where  $S$ , the Huang-Rhys parameter, is a dimensionless measure of the impurity-ion-lattice coupling magnitude.<sup>9</sup>

Figure 3 shows the temperature dependence of the peak widths,  $W(T)$ , extracted from the Gaussian fits to peaks a and b. Statistical errors derived from the fitting procedure are smaller than the plot symbols. The solid and dotted lines represent the best fits of the data to Eq. (2), from which the magnitudes of  $\omega$  and  $S$  were extracted. Vibrational frequencies of peaks a and b are  $1.83 \times 10^{13}$  and  $5.07 \times 10^{13} \text{ s}^{-1}$ , respectively, with corresponding  $S$  values 22.7 and 5.7,  $S > 5$  indicates strong coupling between the impurity ion and lattice and also implies a relatively large Stokes shift;<sup>10</sup> for peaks a and b, the measured shifts are 0.70 and 0.67 eV, respectively. The electron-lattice coupling parameters are summarized in Table I.

### C. Excited-state vibrational energies

The filled symbols in Fig. 4 illustrate the temperature

TABLE I. Electron-lattice coupling parameters for GSO:Ce.

Peak	$W(0)$ (eV)	$\omega$ ( $10^{13} \text{ s}^{-1}$ )	$\omega_{\text{exc}}$ ( $10^{13} \text{ s}^{-1}$ )	$E_2 - E_1$ (eV)	$S$
a	0.135	1.83	4.39	3.30	22.7
b	0.187	5.07	...	...	5.7

dependence of peak a and peak b Gaussian centroids. The statistical error bars are smaller than the plot symbols. Within experimental error, the centroid of peak b is independent of temperature, whereas peak a centroid is shifted to higher energy. There are two plausible explanations for this shift: variations in impurity-ion-ligand separation due to thermal expansion, which affects the Tanabe-Sugano energy-level diagram, and higher-order coupling terms in the electron-lattice interaction.<sup>11</sup>

The excited-state  $5d$  level of the  $\text{Ce}^{3+}$  ion is split into five components by the crystalline electric field, with average splitting 0.35 eV.<sup>10</sup> The energy of the optical absorption transition depends on the strength  $\Delta = 10Dq$  of the crystalline electric field, which, in turn, depends on the distance between the absorbing ions and the nearby ligands. The spatial separation of ions and ligands exhibits temperature dependence through the thermal expansion coefficient. Whether the transition exhibits a shift to higher or lower energy with increasing temperature depends upon the slope  $dE/d\Delta$  of the  $E$  vs  $\Delta$  curve (Tanabe-Sugano energy diagram). A negative slope shifts the optical absorption transition to higher energy with increasing temperature. Unfortunately, we know neither the thermal expansion coefficient nor details of the crystalline electric field (and corresponding Tanabe-Sugano diagram) for  $\text{Ce}^{3+}$  ions in GSO, and thus cannot presently elucidate the contribution of this effect to the centroid shift.

A second well-known temperature effect on absorption band centroids is higher-order coupling terms in the ion-lattice interaction model.<sup>12</sup> Inherent in Eq. (1) is the assumption that average vibrational frequencies of the ground and

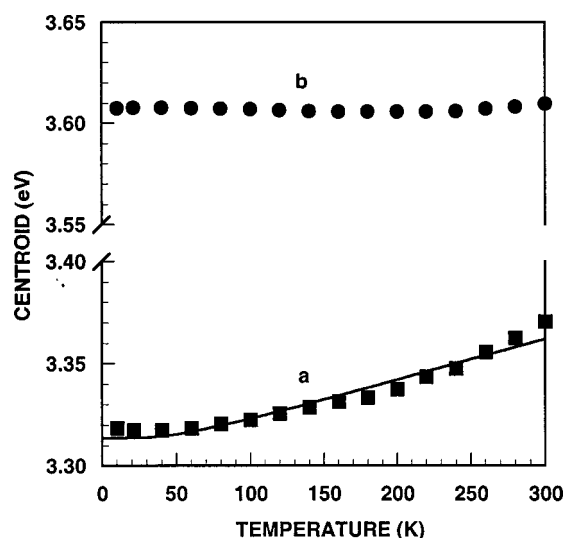


FIG. 4. Temperature dependence of peak a and peak b centroids. The solid line is the best fit of the data to a modified linear model, which includes higher-order, impurity-ion coupling terms in the ion-lattice interaction.

excited states are identical, thus yielding a “linear” model. However, one can include the effects of higher-order coupling by introducing a different frequency,  $\omega_{\text{exc}}$ , for the excited state. The centroid position  $M(T)$  is then given by

$$M(T) = E_2 - E_1 + \frac{1}{4} \hbar \omega \left( \frac{\omega_{\text{exc}}^2}{\omega^2} - 1 \right) \coth \left( \frac{\hbar \omega}{2kT} \right), \quad (3)$$

where  $E_2 - E_1$  is the energy difference between the ground and excited states at the zero position of the configurational coordinate. As illustrated in Fig. 4, peak a exhibits an increase in centroid energy with increasing temperature and approximately obeys Eq. (3) as indicated by the solid line. The vibrational frequency and energy difference obtained from the fit are  $4.39 \times 10^{13} \text{ s}^{-1}$  and 3.30 eV, respectively. A summary of the electron-lattice coupling parameters is given in Table I.

Although the temperature dependence of the centroid is adequately described by Eq. (3), the reader is reminded of the possibility that some fraction of the dependence may be attributed to thermal expansion and its effect on the Tanabe–Sugano diagram, as previously discussed. Presently, we have insufficient data to ascertain the magnitude of these individual effects.

#### D. Absorption band oscillator strengths

The oscillator strength  $f$  characterizing a given optical transition is related to the integrated absorption, index of refraction  $n$ , and concentration of absorbing centers  $N$  by the well-known Smakula formula<sup>13</sup>

$$Nf = 8.21 \times 10^{15} \text{ cm}^{-3} \frac{n}{(n^2 + 2)^2} \int \alpha(E) d(E), \quad (4)$$

where  $\alpha$  is the decadic absorption coefficient in  $\text{cm}^{-1}$  and  $E$  is the energy in eV. For Gaussian absorption bands, as in the present case, the integral is

$$\frac{1}{2} \sqrt{\frac{\pi}{\ln 2}} \alpha_{\text{max}} W \quad (5)$$

with maximum absorption  $\alpha_{\text{max}}$  and full width at half maximum  $W$ . Substituting Eq. (5) into Eq. (4) yields the desired expression

$$Nf = 8.7 \times 10^{16} \text{ cm}^{-3} \frac{n}{(n^2 + 2)^2} \alpha_{\text{max}} W. \quad (6)$$

Calculation of the oscillator strengths of bands a and b requires knowledge of the  $\text{Ce}^{3+}$  concentrations for sites Ce1 and Ce2. GSO formula weight is 422.580 g and density is  $6.71 \text{ g/cm}^3$ , yielding a formula volume of  $1.046 \times 10^{-22} \text{ cm}^3$  (containing two rare-earth sites). The final  $\text{Ce}^{3+}$  concentration is a product of melt concentration (0.25 at. %) and segregation coefficient (0.6). However, this computed concentration (0.15 at. % relative to  $\text{Gd}^{3+}$ ) is not uniformly distributed between the two crystallographically inequivalent sites. But, knowledge of the distribution can be obtained from the work of Suzuki *et al.*<sup>5</sup> on GSO of the same stated concentration. By adding the emission spectrum of Ce1 (excited at 345 nm) to the spectrum of Ce2 (excited at 378 nm) in the ratio of 58:42, they calculated an emission spectrum at

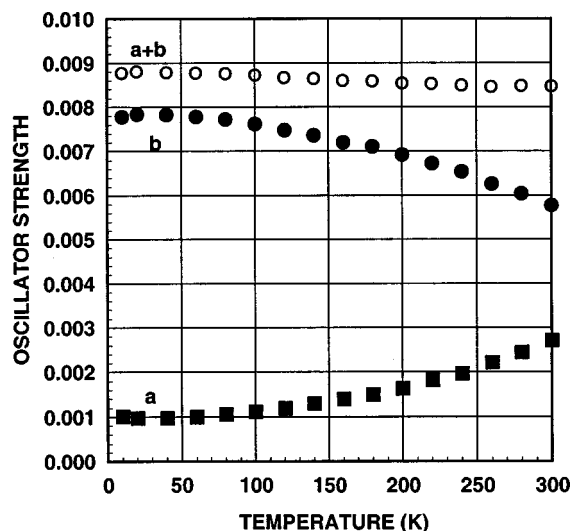


FIG. 5. Temperature dependence of a and b band oscillator strengths. Note their sum ( $a+b$ ) is nearly temperature independent. These bands are identified as seven- and nine-oxygen-coordinated sites, respectively.

11 K that mimicked the experimental one. This ratio ought to correspond to the ratio of concentrations for the two sites. Accordingly, we assigned the  $\text{Ce}^{3+}$  distribution as 58% to site Ce1 and 42% to site Ce2 and calculated concentrations of  $8.35 \times 10^{18}$  and  $6.02 \times 10^{18} \text{ cm}^{-3}$ , respectively.

With known  $\text{Ce}^{3+}$  concentrations, average index of refraction ( $n=1.85$ ), and measured Gaussian absorption, we computed the oscillator strengths of the two bands as a function of temperature and display the results in Fig. 5. Each oscillator strength exhibits moderate temperature dependence with inversely related slopes. This dependence is a measure of the absorption band area because concentration and index of refraction are assumed to be temperature independent. Note the sum of oscillator strengths ( $a+b$ ) is nearly temperature independent, implying temperature independence of the combined peak area. The striking feature of the data, however, is the much larger  $f$  value of peak b relative to peak a, approximately a factor of 8 and 2 at 10 and 300 K, respectively. This result suggests the two peaks belong to different Ce sites as proposed by Suzuki *et al.*<sup>5</sup> Williams *et al.*<sup>14</sup> have compiled a comparison of experimental and theoretical  $4f \rightarrow 5d$  oscillator strengths for  $\text{Ce}^{3+}$  ions in various host lattices.

#### E. $\text{Ce}^{3+}$ site identification

The impurity-ion-lattice coupling parameters of absorption bands a and b in GSO are strikingly different in magnitude and temperature dependence, indicative of distinctly different  $\text{Ce}^{3+}$  sites. Suzuki *et al.*<sup>5</sup> previously established that peaks a and b are correlated with substitutional sites Ce2 and Ce1, respectively, but could not identify them as being seven- or nine-oxygen coordinated. The present data, when coupled with previous results of Williams *et al.*,<sup>14</sup> strongly suggest that sites Ce1 and Ce2 are nine- and seven-oxygen coordinated, respectively. Williams *et al.* noted that variations in  $f$  are correlated with the average  $\text{Ce}^{3+}$ -ion-ligand distance, with a smaller separation corresponding to a



smaller  $f$  value relative to the free-ion magnitude. This correlation most likely arises from the differential radial expansion of the overlapping rare-earth and ligand orbitals, which leads to a greatly reduced dipole matrix element in the quantum mechanical oscillator strength expression. To see this more clearly, we express  $f$  in quantum mechanical terms

$$f_{nm} = \frac{8\pi^2 m \nu_{nm} |\langle n | \mathbf{M} | m \rangle|^2}{3e^2 h}, \quad (7)$$

where  $\nu_{nm}$  is the transition frequency between the states  $n$  and  $m$ , and  $|\langle n | \mathbf{M} | m \rangle|^2$  is the squared dipole matrix element between the two states.  $\mathbf{M}$  is the electric dipole moment, which can be expressed in terms of charge density  $\rho(\mathbf{r})$  and electron charge  $e$

$$\mathbf{M} = e \int \rho(\mathbf{r}) \mathbf{r} d\tau \quad (8)$$

Insertion of a rare-earth ion into a host lattice causes the rare-earth orbitals to expand radially due to overlap with the ligand orbitals. But the expansion is much greater for  $5d$  orbitals because the inner  $4f$  ones are strongly shielded. This differential expansion leads to a significantly reduced dipole matrix element,  $|\langle 4f | \mathbf{r} | 5d \rangle|$ , and a correlation between oscillator strength and average metal-ion-ligand separation.

As illustrated in Fig. 5,  $f$  values of peak b at all temperatures are considerably larger than those of peak a, implying a larger peak b  $\text{Ce}^{3+}$ -ion-ligand spatial separation. Smolin and Tkachev<sup>6</sup> elucidated the structure of GSO and obtained Gd–O distances for Gd in the seven- and nine-oxygen-coordinated sites as 2.39 and 2.49 Å, respectively; similar ion-ligand distances are expected for  $\text{Ce}^{3+}$  ions in GSO. These results, combined with the oscillator strength-separation correlation and our present oscillator strength data, suggest that peak a is correlated with the seven-oxygen-coordinated site, previously labeled site Ce2, and peak b is identified as the nine-oxygen-coordinated site, previously labeled site Ce1. These results strongly support the two-center model previously proposed by Suzuki *et al.*<sup>5</sup>

#### IV. SUMMARY

In summary, we have measured the uv-vis optical absorption of GSO in the regime 10–300 K and analyzed the two principal absorption bands whose maxima at 10 K are 3.32 eV (peak a) and 3.61 eV (peak b). The bands are well described by Gaussian line shapes and are in excellent agreement with previously reported results. The linear model of impurity-ion-lattice coupling adequately describes the tem-

perature dependence of absorption band widths. Huang-Rhys parameters of peaks a and b are 22.7 and 5.7, respectively, indicating strong ion-lattice coupling and relatively large Stokes shifts ( $\sim 0.7$  eV). Extracted quantum vibrational frequencies are  $1.83 \times 10^{13} \text{ s}^{-1}$  (peak a) and  $5.07 \times 10^{13} \text{ s}^{-1}$  (peak b). Peak b centroid is nearly temperature independent, whereas peak a centroid exhibits a shift to higher energy with increasing temperature. Although this shift can be well described by including higher-order coupling terms in the ion-lattice interaction, contributions from crystal-field effects cannot be excluded.

Oscillator strengths of the two bands were calculated from Smakula's formula, combined with knowledge of the cerium concentration for the two crystallographically inequivalent sites. From 10 to 300 K peak a  $f$  values ranged from  $(9.8 \text{ to } 26.8) \times 10^{-4}$ , and peak b  $f$  values varied from  $(7.8 \text{ to } 5.8) \times 10^{-3}$ . Based on the observation of Williams *et al.*<sup>14</sup> that larger oscillator strengths imply a larger metal-ion-ligand separation, we have identified sites Ce1 (peak b) and Ce2 (peak a) as the nine- and seven-oxygen-coordinated sites, respectively. These results strongly support the conclusion of Suzuki *et al.*<sup>5</sup> that these bands are correlated with the two crystallographically inequivalent substitutional cerium sites in GSO.

#### ACKNOWLEDGMENTS

This research was supported by the U.S. Department of Energy and administered by the University of California.

<sup>1</sup>K. Takagi and T. Fukuzawa, Appl. Phys. Lett. **42**, 43 (1983).

<sup>2</sup>H. Ishibashi, Nucl. Instrum. Methods Phys. Res. A **294**, 271 (1990).

<sup>3</sup>H. Suzuki, T. A. Tombrello, C. L. Melcher, and J. S. Schweitzer, IEEE Trans. Nucl. Sci. **41**, 681 (1994).

<sup>4</sup>H. Suzuki, T. A. Tombrello, C. L. Melcher, and J. S. Schweitzer, J. Lumin. **60–61**, 963 (1994).

<sup>5</sup>H. Suzuki, T. A. Tombrello, C. L. Melcher, and J. S. Schweitzer, Nucl. Instrum. Methods Phys. Res. A **320**, 263 (1992).

<sup>6</sup>Y. I. Smolin and S. P. Tkachev, Sov. Phys. Crystallogr. **14**, 14 (1969).

<sup>7</sup>G. B. Loutts, A. I. Zagumennyi, S. V. Lavrishchev, Y. D. Zavartsev, and P. A. Studenikin, J. Cryst. Growth **174**, 331 (1997).

<sup>8</sup>C. C. Klick and J. H. Schulman, in *Solid State Physics*, edited by F. Seitz and D. Turnbull (Academic, New York, 1957), Vol. 5, p. 97.

<sup>9</sup>K. Huang and A. Rhys, Proc. R. Soc. London, Ser. A **204**, 404 (1950).

<sup>10</sup>G. Blasse and B. C. Grabmaier, *Luminescent Materials* (Springer, Berlin, 1994).

<sup>11</sup>B. DiBartolo, *Optical Interactions in Solids* (Wiley, New York, 1968).

<sup>12</sup>A. E. Hughes and B. Henderson, in *Point Defects in Solids*, edited by J. H. Crawford and L. M. Slifkin (Plenum, New York, 1972), Vol. 1, p. 291.

<sup>13</sup>A. Smakula, Z. Phys. **59**, 603 (1930).

<sup>14</sup>G. M. Williams, N. Edelstein, L. A. Boatner, and M. M. Abraham, Phys. Rev. B **40**, 4143 (1989).